# TMD Stroke Limiting Influence on Barge-type Floating Wind Turbines

D. Villoslada*
University Complutense of Madrid, Computer Sciences Faculty, 28040-Madrid, Spain
davillos@ucm.es

M. Santos
Institute of Knowledge Technology, University Complutense of Madrid, 28040-Madrid, Spain
msantos@ucm.es

M. Tomás-Rodríguez
The City, University of London, London, UK.
Maria.Tomas-Rodriguez.1@city.ac.uk

* Corresponding author: Daniel Villoslada. Computer Sciences Faculty, C/ Profesor García Santesmases 9, UCM, 28040-Madrid, Spain. Email: davillos@ucm.es

**Abstract.**

In this paper, passive structural control techniques are applied to a barge-type Floating Offshore Wind Turbine (FOWT) to mitigate the impact of pendulum effect loads. The passive structural control device, a tuned mass damper (TMD) installed in the nacelle, is analyzed on a reduced dynamics FOWT model. Genetic algorithms are used for the optimization process, taking the tower fatigue as the fitness function, implemented as the standard deviation of the fore-aft tower top displacement. The optimization of the TMD shows that its resulting stroke is unfeasible in terms of space needed for installation. Therefore, the addition of stroke-limiting stops to the TMD should be considered. A new optimization, including stops, yields a clear improvement of the device performance while limiting the stroke to the nacelle dimensions. It is observed that the stops allow to mitigate the second collective platform pitch-tower bending mode in addition to the first one. Finally, a third case is presented, considering the whole stops configuration as additional variables in the optimization loop. This last case improved the TMD performance in terms of vibration suppression rate, proving the effectiveness of optimizing stops for mass and space constrained applications.

**Keywords:** Barge-type floating offshore wind turbine, passive structural control, optimization, genetic algorithms, TMD stroke, stops.

## 1 Introduction

Wind is a renewable source of energy that is efficiently helping to mitigate climate change negative impact. This clean energy reduces environmental pollution by replacing other more polluting resources, such as fossil energy (Mikati et al., 2013). But the field of onshore wind turbines (WT) seems to have reached a high degree of exploitation and technological maturity. To expand the harnessing of the wind to more promising areas, offshore wind turbines started to be developed a few decades ago (Costoya et al., 2020). Initially, coastal wind turbines were installed in shallow waters, where winds were stronger and more stable (Caglayan et al., 2019). Nevertheless, the deployment and maintenance of these turbines is implied high costs, whilst they do not really solve the problem of acoustic and visual impact, neither some negative effects on marine animals and birds, and they affect tourism and property values. These are some of the reasons that have triggered the installation of wind farms in deeper waters.

Conventional offshore wind turbines are installed on fixed foundations laying on the seabed, making them unsuitable for waters more than 50 m deep. As an alternative, floating wind turbines (FOWT) are offshore WTs mounted on a floating structure that allows the turbine to generate electricity in deep waters in comparison to the traditional bottom-fixed ones. In addition, the cost of installation is reduced as assembly is simplified, deployment is more flexible, inspections and maintenance are easier, and the environmental impact is reduced. FOWTs not only allow to diminish the acoustic and visual impact, but also reduce the seabed footprint and so the damage to the abundant coastal flora and fauna. An increasing industrial and commercial interest in these types of energy harvesting systems is observed nowadays.

Floating offshore wind turbines use new concepts of foundation, which are technically feasible for its deployment on waters from 60 to 900 meters depth. FOWTs are divided into three major types, depending on the restoring mechanism they rely on. The main stabilizing methods are buoyancy, ballasting, and

mooring. The derived floating foundation types are the barge, the spar buoy, and the tension leg platform (Wang et al., 2010).

The present study focuses on barge-type floating wind turbines, which stand out for their simple design, assembly, and maintenance benefits. The stability of this concept is achieved through its waterplane area moment and the mooring forces from the catenary lines.

Preliminary load analysis carried out by Jonkman and Buhl (2007) on a wind turbine installed on a barge-type floating platform. It was shown that waves and wind induced motions that increased the displacements and loads on the structure due to an inverted pendulum effect. Even more, the relative structural fatigue between the sea-based and land-based turbines increases from the blade tip to the tower base, reaching unacceptable figures.

A promising approach to reduce FOWT loads is the application of structural control, which have been successfully used for decades in civil engineering to protect structures from damage caused by dynamic loading such as earthquakes, wind, or traffic (Saaed et al., 2015). The application of these control devices to offshore wind turbines has been a topic of interest the last years (Yang et al., 2019a). Structural control can be considered as an additional Degree of Freedom (DOF) added to the structure, instead of an intervention of the existing turbine power control system. If sufficient, the main benefit of the structural control application would be not to require any design alteration from the baseline land-based wind turbine.

Among the three major types of structural control, which are passive, semi-active, and active, this work focuses on the passive approach. Within this type, energy dissipation devices are the ones of interest and, more specifically, the dynamic vibration absorbers (DVA). They typically consist of a mass resonant device attached to the structure by a spring and a viscous damper (Tomás-Rodríguez and Santos, 2019). This combination is usually referred to as a Tuned Mass Damper (TMD). The tuning of the TMD parameters is a crucial process, typically carried out by adapting the spring stiffness and the damper constant to bind the TMD resonance frequency to one of the system natural frequencies, which maximizes energy absorption (Yang et al., 2019a).

The effectiveness of a TMD device is directly proportional to its mass (Stewart and Lackner, 2013). However, the more massive the TMD is, the longer its stroke and thus, more room is required for its installation. In order to consider the space limitations of the nacelle, where these devices are usually installed, stops are introduced in the form of additional springs and dampers at both ends. This generates nonlinearities, giving rise to a more complex dynamics of the system. Moreover, in the case of limiting stops being present, the tuning of the stop devices may be considered as additional variables to be optimized. This results in a larger optimization problem that, to the best of the authors' knowledge, has not been addressed before in other studies.

In order to provide plausible and practical solutions, this work analyses the feasibility of passive structural control in barge-type FOWTs. Reducing the platform oscillations and structural vibrations improves the system's efficiency and decreases the structural fatigue. Therefore, a TMD is installed in the nacelle. Using a reduced dynamic FOWT model, the TMD is optimized to reduce the collective platform pitch-tower bending mode of the floating turbine. The design process adds stops that limit the TMD stroke to fit it into the nacelle. As the addition of stops to the TMD modifies the system's dynamics, various optimizations were carried out to analyze the dependency of the wind turbine efficiency with respect to the stops configuration and, besides, to study the energy absorption in the frequency and time domain.

Another interesting contribution of this work is the inclusion of the TMD stops in the mathematical model of the FOWT. Indeed, the novelty of this work lies in the fact that usually stops are not considered as part of the TMD passive control, and when they are included, the optimization of the stroke of the TMD is carried out independently from the wind turbine behaviour. In this paper, equations have been obtained to represent the action of these stops on the dynamics of the floating wind turbine.

Simulation experiments have been carried out on the 5-MW NREL (National Renewable Energy Laboratory) barge-type floating wind turbine, using FAST-SC (Fatigue, Aerodynamics, Structures, and Turbulence), the high-fidelity simulation software developed by Lackner and Rotea (2011b), that includes structural control functionalities. Interesting and novel conclusions have been obtained regarding the mitigation of the main frequency modes of the floating device.

109 This paper is organized as follows: Section 2 summarizes some related works. The reduced model of
110 the floating wind turbine used is described in Section 3. The passive structural control device, including the
111 stops, is also modelled in this section. Section 4 shows the optimization process for tuning the TMD
112 parameters. In Section 5 the optimization of the TMD with stops under different configurations is presented.
113 Results are discussed. The paper ends with the conclusions and suggestions for future works.

114 **2 Related works**

115 Although relatively recent, the field of FOWT has already gathered a substantial amount of research
116 devoted to improving the efficiency of these type of systems (Lackner and Rotea, 2011b). The approaches
117 taken in the current existing literature cover a wide range of areas of specialization, depending mainly on
118 the objectives to be achieved (Pimenta et al., 2020). The general goal has been to provide a robust and
119 maximized energy production (Olondriz et al., 2019; Rubio et al., 2019; Sierra-García and Santos, 2020a;
120 Sierra and Santos, 2021). More specifically, the application of structural control to offshore wind turbines
121 has been a topic of interest the last years (Sierra-García and Santos, 2020b; Park et al., 2019; Zuo et al.,
122 2020). Passive control devices have started to be widely applied yielding good results in terms of load
123 mitigation and vibration control.

124 In Lackner and Rotea (2011a), passive and active control were investigated for a floating barge-type
125 wind turbine. Optimal parameters are determined using a parametric study of the tuned mass damper device.
126 The performance was evaluated as a function of the active power consumption and the stroke of the
127 actuator. The obtained results showed that active control is effective in reducing structural loads, but at the
128 expense of active power and large strokes. Also (Lackner and Rotea, 2011b) applied two TMDs located in
129 the nacelle of the turbine model, with one TMD in the fore-aft direction, and the other in the side-side
130 direction. The stiffness, damping and external force of each TMD were controllable. An analysis was done
131 to determine the optimal parameters of a passive single DOF, fore-aft, TMD system in both a barge-type
132 and monopile support structure.

Most of these control devices are installed in the nacelle, although sometimes they are located in the tower of spar-buoy wind turbines (Dinh and Basu, 2015), and much less frequent, in the barge supporting platform (Galán-Lavado and Santos, 2021). In any case, the design of the TMD involves the optimization of its parameters, i.e., stiffness, damping, mass and location, to effectively reduce the vibrations of the wind turbine. To mention a few examples. Stewart and Lackner (2013) used FAST-SC to assess passive control solutions for both tension leg platforms and barge-type floating wind turbines. They used a TMD located in the nacelle. He et al. (2017) derived a linear model of barge type floating wind turbine with a fore–aft tuned mass damper in the nacelle. The dynamic responses of the wind turbine with/without tuned mass damper were simulated and the suppression effect of the tuned mass damper was investigated over a wide range of load cases. In Liao and Wu (2020), a novel concept of a passive FOWT structure is proposed to overcome the previous limitations of space and mass of tuned mass dampers. The conceptual design was examined on the basis of a finite element model with promising results. In Xie et al. (2019a) a coupled aero-hydro-servo-elastic model of a barge-type wind turbine was developed and simulated for different load cases. An optimized TMD was installed in the nacelle. The time-domain and frequency-domain analysis of simulation results indicated that the designed TMD could significantly inhibit the structural loads and stabilize the electrical output power. Some other studies have considered the stroke as a constraint in the TMD optimization (Yang and He, 2020; Chen et al., 2021). Nevertheless, this work does not use stops to limit the stroke as we propose in here.

At present, the methods to adjust TMD parameters are frequency tuning, genetic algorithms (GA), and surface plot (Yang et al., 2019b). The surface plot approach is usually discarded as it required a considerable computational cost. According to these authors, although the frequency tuning method is an effective approach to find the optimum TMD parameters, it has some limitations. Therefore, the use of GAs to optimize TMD design has grown in recent years. Indeed, Yang et al. (2019b) applied frequency formulas and GA to tune the TMD for the same wind turbine model and obtained a better suppression rate of vibrations with the evolutive technique.

As mentioned, the inclusion of the TMD stops is scarce in the turbine-related literature although some notable exceptions can be found. Hu and He (2017) investigated an active vibration control strategy for a barge-type floating wind turbine by setting a stroke-limited hybrid mass damper (HMD) in the turbine's nacelle. The stroke of the active damper and the active control power consumption were the constraints. Li et al. (2017) used a fore–aft tuned mass damper in the nacelle/tower subsystem to design passive control of a semi-submersible offshore wind turbine. The corresponding mass, stiffness and damping parameters of the TMD in this case were optimized using both exhaustion and genetic algorithm methods, to avoid local minimums. Nevertheless, these studies assumed the stops to be fixed parameters, hence they were not optimized. In Villoslada et al. (2020), the authors explored the addition of a passive inerter parallel-connected to a TMD in the nacelle. Stops were used to limit the stroke, in this case, only the actuation distance was optimized.

Similarly, the work by Park et al. (2019) focused on a magnetorheological damper and its significance on the structural control of a tension leg platform. A parametric study was carried out to determine the optimal parameters of a passive TMD tuned to the first tower natural frequency. The stops were not included in the design process. Xie et al. (2019b) used a single degree of freedom tuned mass damper (TMD) system installed in the platform. To achieve the ideal response mitigation effect, they analyzed the TMD configuration. The stops were not optimized and were fixed. Yang et al. (2019b) also included stops in a TMD model fitted in the platform of a barge-type wind turbine; in this case the stroke was not considered either perhaps due to the fact that space limitation in the platform is not a usual problem.

Cong included the nonlinearity due to space constraints of the wind turbine, which impacts on the vibration control (Cong, 2019). This work studies active tuned mass dampers with constrained stroke in the vibration control of the blades and lateral (side-side) tower vibration of an on-shore wind turbine.

Although the issue of the stroke limitation of TMDs installed in FOWTs is somehow addressed in the literature, for barge-type wind turbines these stops are fixed to a value that –in the best-case scenario- has been obtained from the parametric analysis of the passive control device. Thus, the main difference of the work here presented from those existing previously is that in our case, the optimization process, using

genetic algorithms, includes the stroke in the optimization loop and explores the benefits of including the stops configuration as additional tuning variables.

## 3 FOWT and TMD Model

The baseline floating offshore wind turbine used in this study is the National Renewable Energy Laboratory (NREL) 5-MW wind turbine (Jonkman et al., 2009). It is a horizontal-axis, three-bladed, upwind, variable speed, pitch-controlled turbine with a 126 m rotor diameter and a 90-meter hub height. The main parameters and geometrical properties are summarized in Table 1. This turbine has been adopted as a reference model by many research projects supported by the U.S., the European Union UpWind research program, and the International Energy Agency. It is a rather large rating turbine, whose size was assumed to be the minimum to make a FOWT economically viable, because of the large proportion of costs devoted to the support platform.

The 5-MW wind turbine is mounted on a barge design developed by the Department of Naval Architecture and Marine Engineering at the Universities of Glasgow and Strathclyde under a contract with ITI Energy (Vijfhuizen, 2006). To ensure simplicity in manufacturing, the barge has a squared shape and is ballasted with sea water to achieve the designed draft. Eight catenary lines moor the platform preventing it from drifting. The barge main characteristics are provided in Table 2.

Table 1. Gross properties of the NREL 5-MW Baseline Wind Turbine (Jonkman et al., 2009)

| | |
|---|---|
| Rating | 5 MW |
| Rotor Orientation, Configuration | Upwind, 3 Blades |
| Control | Variable Speed, Collective Pitch |
| Drivetrain | High Speed, Multiple-Stage Gearbox |
| Rotor, Hub Diameter | 126 m, 3 m |

| | |
|---|---|
| Hub Height | 90 m |
| Cut-In, Rated, Cut-Out Wind Speed | 3 m/s, 11.4 m/s, 25 m/s |
| Cut-In, Rated Rotor Speed | 6.9 rpm, 12.1 rpm |
| Rated Tip Speed | 80 m/s |
| Overhang, Shaft Tilt, Precone | 5 m, 5º, 2.5º |
| Rotor Mass | 110,000 kg |
| Nacelle Mass | 240,000 kg |
| Tower Mass | 347,460 kg |
| Coordinate Location of Overall CM | (-0.2 m, 0.0 m, 64.0 m) |

202

203 Table 2. Gross characteristics of the ITI Energy Barge (Vijfhuizen, 2006)

| | |
|---|---|
| Size (W×L×H) | 40 m × 40 m × 10 m |
| Moonpool (W×L×H) | 10 m × 10 m × 10 m |
| Draft, Freeboard | 4 m, 6 m |
| Water Displacement | 6,000 m3 |
| Mass, including Ballast | 5,452,000 kg |
| Center of Mass (CM) below SWL | 0.282 m |
| Roll Inertia about CM | 726,900,000 kg·m2 |
| Pitch Inertia about CM | 726,900,000 kg·m2 |

| | |
|---|---|
| Yaw Inertia about CM | 1,453,900,000 kg·m2 |
| Anchor (Water) Depth | 150 m |
| Separation Between Opposing Anchors | 773.8 m |
| Unstretched Line Length | 473.3 m |
| Neutral Line Length Resting on Seabed | 250 m |
| Line Diameter | 0.0809 m |
| Line Mass Density | 130.4 kg/m |
| Line Extensional Stiffness | 589,000,000 N |

In this paper, the structural control of the barge-type win turbine is implemented by using a tuned mass damper (TMD) system. These devices are very efficient for vibration reduction. They consist on a mass, stiffness elements (springs), and dampers. When a structure vibrates, the fitted TMD vibrates at the same structure's frequency but out of phase. The TMD inertial force reduces the vibrational energy transmitted to the system which dissipates in the form of heat. These systems are referred as "tuned" because the mass and springs are tuned, or adjusted, to the structural mode (i.e. the natural frequency) of the structure to be damped. Usually this is the first vibrational mode (first natural frequency), since it plays the most significant role in a system's response.

Thus, the three configuration parameters of the TMD that much be tuned are:

- Mass, $m_T$ (kg): the larger the TMD mass is, the greater inertia will be and therefore, the greater amount of stored kinetic energy. $m_T$ is usually limited to a ratio of the total mass of the structure.
- Spring stiffness coefficient, $k_T$ (N/m): is defined as the proportionality of the resultant spring force in relation to its compression / extension.

- Damping coefficient, $d_T$ (N·s/m): regulating the magnitude of the resultant force proportional to the relative speed between the ends of the damping element, i.e., between the mass and the structure.

In addition to the above-mentioned parameters, the TMD design process often considers other factors such as:

- TMD position. The TMD can be fitted in any part of the FOWT, i.e., in the nacelle, in the tower or in the platform. The exact location this device will impact the magnitude and frequency of the loads suffered by the TMD, as well as other design constraints.
- TMD orientation: usually referred to a wind-aligned reference system. The most common TMD orientation is fore-aft, which means downwind, or side-side if lateral vibrations are to be considered.
- Stroke limits. Stops can be installed to limit the stroke of the TMD mass. The logic of this action must be also considered.

There are some studies that analyse the dynamical behavior of FOWT depending on the TMD location and the type of floating wind turbine, the later limits the possible locations of the TMD (Dinh and Basu, 2015; Yang et al., 2020). In the case of a barge-type FOWT, the TMD could also be fitted in the platform with the objective of absorbing energy. However, there are three main drawbacks for this approach. First, the platform pitch, although highly energetic in absolute terms, does not display large motions. This means that the installation of a short stroke TMD would require a large mass. Secondly, the orientation of a TMD in the nacelle is always aligned with the fore-aft direction because the nacelle's yaw control turns the rotor towards the upwind direction, whereas if the TMD is fitted in the platform it sustains a steady predetermined direction that not always would be aligned with the external disturbances (wind and waves). Third, it has been shown that the benefits of a TMD fitted on a barge-type FOWT platform are less significant than when this is fitted in the nacelle (Yang et al., 2019b; Galán-Lavado and Santos, 2021). Even in a spar wind turbine, the nacelle TMD optimally tuned is seen to be more effective than the spar TMD (Dinh and Basu, 2015).

242 Several analyses of FOWT have shown that fore-aft oscillations have more influence on tower base
243 loads than side-side oscillations (Jonkman, 2007). In this work, the authors consider the TMD to be fitted
244 in the nacelle and towards the fore-aft direction. A schematic layout is shown in Figure 1.

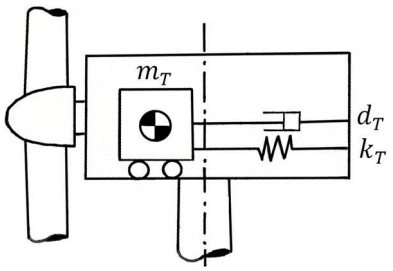


245
246 Figure 1. TMD fore-aft oriented in the nacelle of the floating wind turbine

247 In order to use the 5-MW NREL FOWT as a benchmark, a simple and efficient model is to be included
248 in the optimization loop. A reduced model containing the two fundamental modes of the structure that
249 contribute the most to the tower base loads (Jonkman, 2007) is used in this work. These modes are the
250 platform pitch and the tower fore-aft displacement. The optimization process focuses on tuning the TMD
251 to the collective platform pitch-tower bending modes. No external disturbances (wind or waves) have been
252 considered. The dynamic model of the floating system is obtained by using an Euler-Lagrange approach
253 (see He et al. (2017) for details). The FOWT linear model with the TMD is as indicated in (1). Each of the
254 three differential equations of the model represents the dynamics of one of the rigid solids sub-systems,
255 namely: TMD ($T$ subindex), tower ($t$ subindex), and barge platform ($p$ subindex)

256
$$\begin{cases} I_t\ddot{\theta}_t = m_t g R_t \theta_t - k_t(\theta_t - \theta_p) - d_t(\dot{\theta}_t - \dot{\theta}_p) \\ \quad -m_T g(R_T\theta_t - x_T) - k_T R_T(R_T\theta_t - x_T) \\ \quad -d_T R_T(R_T\dot{\theta}_t - \dot{x}_T) \\ I_p\ddot{\theta}_p = -d_p\dot{\theta}_p - k_p\theta_p - m_p g R_p\theta_p \\ \quad +k_t(\theta_t - \theta_p) + d_t(\dot{\theta}_t - \dot{\theta}_p) \\ m_T\ddot{x}_T = k_T(R_T\theta_t - x_T) + m_T g\theta_t \\ \quad +d_T(R_T\dot{\theta}_t - \dot{x}_T) \end{cases} \quad (1)$$

257 This model has three degrees of freedom (DOF): platform pitch angle ($\theta_p$), tower bending angle ($\theta_t$)
258 and TMD deviation distance, $x_T$, the latter regarding the barge and tower absolute rest position, that is also
259 known as the (fore-aft) tower top displacement. The $R_i$ terms represent the distances from the center of

mass of each element to the tower-platform virtual hinge point. The tower's flexibility and platform's hydrodynamic properties are modeled by a pair of springs, $k_t$, $k_p$ (N/m), and dampers, $d_t$, $d_p$ (N·s/m). A complete diagram of the system's model is shown in Figure 2.

This dynamic model must be characterized for each specific wind turbine through an identification process in order to obtain the values of the different coefficients. Due to the lack of available real data, the identification of the model parameters was carried out using synthetic data generated by the simulation of the floating wind turbine with the aeroelastic computer-aided engineering tool FAST-SC. This software allows to generate the wide range of data sets necessary for the identification and validation of the model. These data sets were obtained under different conditions to obtain solutions with different configurations. The least squares Levenberg-Marquardt algorithm was used for this identification process, taking as input FAST free decay tests of 100 secs duration, having the platform an initial pitch angle of 3º. After evaluating the identification and validation results in three phases (algorithm, test duration, and initial platform pitch selection), the best estimate of the model parameters is obtained. A more detailed description of this methodology can be found in Villoslada et al., 2021. The identified parameters were the spring stiffness *k* (N/m), damping coefficient *d* (N·s/m), and the inertia moment *I* (kg·m$^2$), for both the platform (*p* subindex) and turbine (*t* subindex), that is, $k_p$, $k_t$, $d_p$, $d_t$, $I_p$, and $I_t$. Their identified values are listed in Table 3.

Table 3. Identified parameters of the reduced FOWT dynamics model.

| $k_t$ (N/m) | $k_p$ (N/m) | $d_t$ (Ns/m) | $d_p$ (Ns/m) | $I_t$ (kg·m$^2$) | $I_p$ (kg·m$^2$) |
|---|---|---|---|---|---|
| $1.4635 \cdot 10^{10}$ | $2.0016 \cdot 10^{9}$ | $2.5415 \cdot 10^{7}$ | $5.6431 \cdot 10^{7}$ | $3.4523 \cdot 10^{9}$ | $2.1613 \cdot 10^{9}$ |

This model was validated with the corresponding one in FAST, and implemented in Matlab so the optimal parameters of the passive control devices can be found.

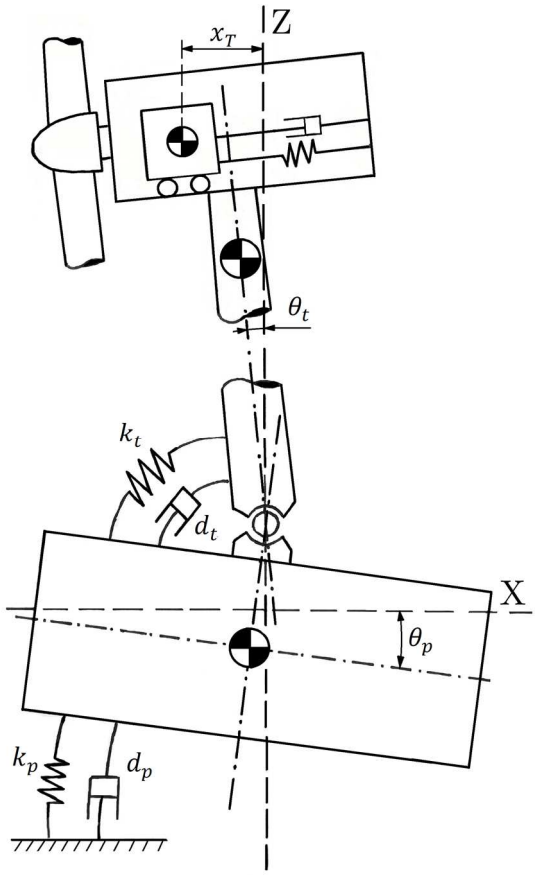


Figure 2. FOWT model diagram

### 3.1 Addition of stops to the FOWT TMD model

TMD stops limit the resonant mass stroke. These are used to take into account the available space of the stroke of a TMD, thus to make the TMD installation feasible and realistic. These stops are usually implemented as a combination of additional spring and damper that start to act when the mass deviates a certain distance with respect to its rest position. A diagram of a TMD with stops is shown in Figure 3.

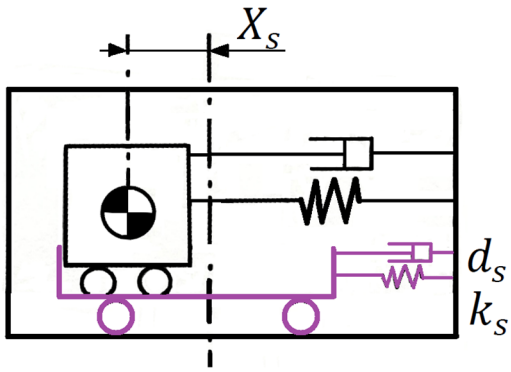


Figure 3. TMD with stops

The TMD stops can be characterized by three parameters, which in this case have been selected to ensure compatibility with the ones used in FAST-SC. Although FAST-SC allows to configure every stop independently, in our scenario the same configuration is applied for both stops, the upwind and the downwind stops (as if there were a single pair of spring-damper acting at both ends, see Figure 3). The stops parameters are:

- $X_s$ (m): stops actuation distance, measured from the rest position. In FAST-SC, it corresponds to variables TmdXDWSP and TmdXUWSP, upwind and downwind respectively.
- $k_s$ (N/m): stop spring stiffness. In FAST-SC it corresponds to variable TmdXSSpr.
- $d_s$ (N·s/m): stop damping coefficient. In FAST-SC it corresponds to variable TmdXSDamp.

In addition to the definition of the forces exerted by the stops, attention must be paid to its operational logic. The same performance implemented in FAST-SC, which was empirically deduced, has been simulated. In conclusion, the stops can only apply restoring forces on the mass. The spring always acts and the damper only works when the mass is moving away from its rest position.

Considering each stop device independently, the new terms to be added to the model dynamics were obtained. In the case of the stop spring, a restoring potential force is obtained whenever the mass position exceeds the actuation distance ($X_s$). Therefore, the spring modifies the system potential energy $\Delta T$ according to the following expression:

$$\boldsymbol{\Delta T} = \begin{cases} +\frac{1}{2}\boldsymbol{k_s}[(\boldsymbol{R_T sin\theta_t - x_T}) + \boldsymbol{X_s}]^2 & \boldsymbol{if\ (R_T sin\theta_t - x_T) < -X_s} \\ +\frac{1}{2}\boldsymbol{k_s}[(\boldsymbol{R_T sin\theta_t - x_T}) - \boldsymbol{X_s}]^2 & \boldsymbol{if\ (R_T sin\theta_t - x_T) > X_s} \end{cases} \quad (2)$$

This potential energy variation affects the system generalized coordinates, $\theta_t$ and $x_T$, as follows:

$$\frac{\partial \Delta T}{\partial \theta_t} = \begin{cases} -\boldsymbol{k_s R_T cos\theta_t (R_T sin\theta_t - x_T + X_s)} & \boldsymbol{if\ (R_T sin\theta_t - x_T) < -X_s} \\ -\boldsymbol{k_s R_T cos\theta_t (R_T sin\theta_t - x_T - X_s)} & \boldsymbol{if\ (R_T sin\theta_t - x_T) > X_s} \end{cases} \quad (3)$$

$$\frac{\partial \Delta T}{\partial x_T} = \begin{cases} -\boldsymbol{k_s (x_T - R_T sin\theta_t - X_s)} & \boldsymbol{if\ (R_T sin\theta_t - x_T) < -X_s} \\ -\boldsymbol{k_s (x_T - R_T sin\theta_t + X_s)} & \boldsymbol{if\ (R_T sin\theta_t - x_T) > X_s} \end{cases} \quad (4)$$

These expressions can be simplified for small angles as:

$$\frac{\partial \Delta T}{\partial \theta_t} = \begin{cases} -\boldsymbol{k_s R_T (R_T \theta_t - x_T + X_s)} & \boldsymbol{if\ (R_T sin\theta_t - x_T) < -X_s} \\ -\boldsymbol{k_s R_T (R_T \theta_t - x_T - X_s)} & \boldsymbol{if\ (R_T sin\theta_t - x_T) > X_s} \end{cases} \quad (5)$$

$$\frac{\partial \Delta T}{\partial x_T} = \begin{cases} -\boldsymbol{k_s (x_T - R_T \theta_t - X_s)} & \boldsymbol{if\ (R_T sin\theta_t - x_T) < -X_s} \\ -\boldsymbol{k_s (x_T - R_T \theta_t + X_s)} & \boldsymbol{if\ (R_T sin\theta_t - x_T) > X_s} \end{cases} \quad (6)$$

In the case of the stop damper, a non-conservative force acts on the mass. This force is only restoring, so it is only applicable when the mass is moving away from the rest position. This changes the non-potential forces in the following way:

$$\begin{cases} \boldsymbol{\Delta Q_{\theta_t} = -d_s R_T (R_T \dot{\theta}_t cos\theta_t - \dot{x}_T)} \\ \boldsymbol{\Delta Q_{\theta_p} = 0} \\ \boldsymbol{\Delta Q_{x_T} = d_s (R_T \dot{\theta}_t cos\theta_t - \dot{x}_T)} \end{cases} \quad (7)$$

Comparing equations (1) and (7), the damper can be implemented in the model by adding the stop damping coefficient ($d_s$) to the one of the TMD ($d_T$). The stop damper will act whenever one of the following position and velocity conditions are satisfied:

$$\begin{cases} \boldsymbol{(R_T sin\theta_t - x_T) < -X_s \vee (R_T \dot{\theta}_t cos\theta_t - \dot{x}_T) < 0} \\ \boldsymbol{(R_T sin\theta_t - x_T) > X_s \vee (R_T \dot{\theta}_t cos\theta_t - \dot{x}_T) > 0} \end{cases} \quad (8)$$

## 4 Optimization case 1: TMD without stops

The FOWT model described in (1) is included in an optimization loop to tune the TMD parameters. The standard deviation of the Tower Top Displacement in the fore-aft direction, σ(TTD or σ($TTD_{FA}$), was used as fitness function of the genetic algorithm optimization solver. According to other works in the field, the standard deviation of the tower top fore-aft deflection, σ(TTD) is the most used variable in the TMD optimization, since variability in $TTD_{FA}$ correlates strongly with fatigue loads in the tower (Lackner and Rotea, 2011b).

Genetic algorithms have been used to find the optimal TMD device parameters as they have been proved efficient in many similar applications (Alonso-Zotes and Santos Peñas, 2010). All the optimization processes were implemented in Matlab. The configuration of the GA here applied has a population size of 50 individuals, rank scaling, stochastic uniform selection with a crossover probability of 0.8, and a mutation probability of 0.01.

Each optimization case was set up within an interval for the values of the parameters to be optimized in order to narrow the search space, so that to ensure convergence and to accelerate the optimization. In addition, a different resolution for each variable was specified to improve the sensitivity of the optimization for those variables impacting most the performance. The variation in resolutions allowed to limit the search space and thus achieving faster convergence of the genetic algorithms. For example, spring stop stiffness may have lower resolution than TMD spring stiffness. A wide variety of resolution and search space settings were tested and adapted for each specific scenario, carrying out various optimization rounds with a low resolution, using a wider search space, and then with higher resolution, in a narrower search space.

To explore the advantages and disadvantages of including stops in the TMD, an optimization was run in the first place without considering the stops, as baseline (referred to as case 1). That sets an optimization problem with only two variables: $k_T$ [N/m] and $d_T$ [N·s/m].

Moreover, initially the TMD mass was considered as an optimization variable, but it was found that the optimal solution always tends to the maximum value (Lackner and Rotea, 2011b). Thus, it was fixed to

different values. Table 4 shows the TMD best parameters for different mass values, including information about the performance in terms of suppression rate (%), and the resulting stroke (m). The suppression rate is the ratio of σ(TTD) reduction with respect to the system response without any structural control with the same simulation conditions (100 s, 5º free decay platform pitch). Higher suppression rate means higher vibrations absorption. The two bolded values of the mass will be used for the next experiments for comparison purposes.

Table 4. Optimization results of the TMD without stops

| $m_T$ (kg) | $k_T$ (N/m) | $d_T$ (N·s/m) | *Suppression Rate* (%) | *Stroke* (m) |
|---|---|---|---|---|
| 5,000 | 1,246 | 268 | 25.5 | 49.32 |
| 10,000 | 2,424 | 881 | 30.06 | 33.63 |
| **20,000** | **4,568** | **2,636** | **34.73** | **23.57** |
| 30,000 | 6,568 | 5,436 | 37.65 | 18.54 |
| **40,000** | **8,292** | **9,766** | **40.06** | **14.27** |
| 50,000 | 9,693 | 14,983 | 42.27 | 11.39 |
| 60,000 | 11,123 | 21,812 | 44.32 | 9.07 |

The limits and resolution used for the optimization case 1 are shown in Table 5.

Table 5. Limits and resolution for optimization case 1

| Variable | Resolution | Low limit | High limit |
|---|---|---|---|
| $k_T$ (N/m) | 1 | 0 | $10^5$ |
| $d_T$ (N·s/m) | 1 | 0 | $10^5$ |

The FOWT response with the optimized $m_T = 40{,}000$ kg in comparison to the system without TMD is shown in Figure 4. The platform pitch (Figure 4, bottom) is completely stabilized in 35 s with the passive

356 control, whereas without TMD the platform continues oscillating for 800 s. Regarding the Tower Top
357 Displacement (TTDspFA) (Figure 4, top), which is composed of two vibration modes, it is possible to see
358 that the first dominating mode (related to the platform pitch mode) is damped out substantially more than
359 the second mode (related to the tower bending mode). This will be later discussed using the spectral analysis
360 of the TTD variable.

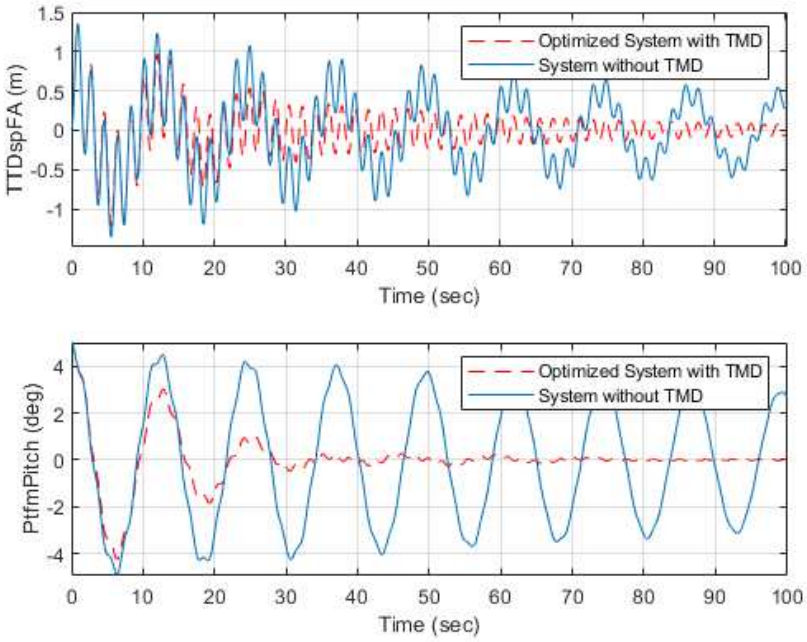


361

362 Figure 4. Simulation of the FOWT with optimized 40 ton TMD (red) and without TMD (blue). Tower
363 Top Displacement TTDspFA (top) and Platform Pitch PtfmPitch (bottom).

364 Some authors adjust the spring stiffness coefficient so that the natural undamped frequency of the TMD
365 is equal to the first collective platform pitch-tower bending mode (Yang et al., 2019b). This first mode is
366 the platform pitch mode and has a frequency of about $w_n$=0.086 Hz, so the corresponding spring stiffness
367 for a 40,000 kg TMD would be 11,680 N/m. Although this is a good practice, it seems more convenient to
368 include the stiffness as another variable in the optimization loop to find the best value that guarantees a
369 global optimum solution to minimize the σ(TTD). Therefore, the TMD will be optimally tuned not only to
370 reduce the first collective platform pitch-tower bending mode, but also the second mode.

As already stated, the TMD performance is directly related to its mass. There is an inverse correlation between the mass and the resulting stroke. In Figure 5, the stroke length decreases logarithmically with the increase of the TMD mass. However, considering that the nacelle is 18 m long, the stops are necessary. Note that the stroke length is calculated from the rest position to the maximum separation, so the physical space required for a real implementation of the control device would be at least twice the mentioned stroke.

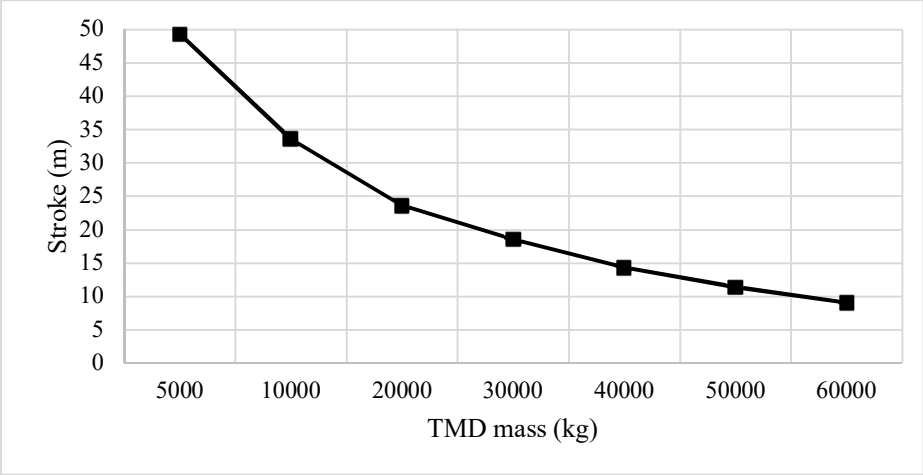


Figure 5. Relation between TMD stroke and mass

## 5 Optimization of TMD with stops

In order to install the TMD in the nacelle, the dimensions of this structural control system including the stops must be considered as a constraint in the TMD optimization. This introduces non-linear dynamics to the model and three new optimization variables: the distance respect to rest position from which the stops start to act, $X_s$ (m), and its spring and damper coefficients, $k_s$ (N/m) and $d_s$ (N·s/m) (Figure 3). The TMD non-linearities arise because the stops only act if the mass is displaced from its rest position more than $X_s$. Moreover, the stop damper only works when the mass is moving away from its rest position.

As in the previous case, the FOWT model was included in the optimization loop, with the fatigue given by the standard deviation of the TTD, i.e., using σ(TTD) as the fitness function. The system was evaluated for free decay tests, with initial platform pitch of 5º. Simulation time is 100 s. In order to address the space

limitation constraints, a stroke penalty was added to the fitness function F (9) to limit those solutions exceeding the defined maximum stroke, $stroke_{max,}$. That is, the stroke penalty is defined to limit the maximum stroke of the TMD while allowing the genetic algorithm to optimize the stops position. This penalty factor is introduced after confirming that the required unrestricted stroke for a specific case is higher than the installation space available. Therefore, the stroke penalty allows to discard unfeasible solutions.

$$F = \sigma(TTD) \cdot \left(\frac{10 \cdot stroke}{stroke_{\max}}\right) \; if \; stroke > stroke_{max} \qquad (9)$$

The configuration of the GA is the same as in the previous experiment, that is, population size of 50 individuals, rank scaling, stochastic uniform selection with crossover probability of 0.8, and mutation probability of 0.01.

The TMD mass, $m_T$, is not used as an optimization variable as explained before. Two different mass values were selected for the experiments, according to the mass ratios used in other works: 20,000 kg and 40,000 kg. These masses represent 2.8 % and 5.7 % of the wind turbine mass and 0.33 % and 0.65 % of the total mass including the barge platform.

Two different scenarios were considered, combining the TMD optimization process and the stops:

- Case 2: Optimization of the TMD parameters considering fixed stops. Variables: $k_T$ and $d_T$.
- Case 3: Optimization of the TMD parameters and the stops configuration. Variables: $k_T$, $d_T$, $X_s$, $k_s$ and $d_s$.

### 5.1 Optimization case 2: TMD with fixed stops

In this case 2, stops are not considered in the optimization loop. That is, the stops are fixed and only the TMD parameters are optimized. The values of the stops are as proposed in Lackner and Rotea (2011b), which have been used in this work as a reference to validate and compare the results. The stop actuation distance ($X_s$) was set to 8 m and the spring stiffness ($k_s$) and damper coefficient ($d_s$) were set to $5 \cdot 10^5$ N/m and $5 \cdot 10^5$ N·s/m, respectively.

Table 6 shows the optimum values and the performance measurements for the two different masses selected, and the reference solutions proposed by other authors. To avoid biases due to the use of a different model from the one used in the reference studies, and in order to make a fair comparison, the suppression rate and stroke were obtained using FAST-SC software (same model for all, free decay test with 5º of platform pitch, and simulation time of 100 s).

Table 6. Optimization case 2. Solutions and performance

| | $m_T$ (kg) | $k_T$ (N/m) | $d_T$ (Ns/m) | *Suppression Rate* (%) | *Stroke* (m) |
|---|---|---|---|---|---|
| Lackner and Rotea (2011b) | 20,000 | 5,000 | 9,000 | 27.49 | 8.096 |
| Own | 20,000 | 1,423 | 5,685 | 30.38 | 8.191 |
| Stewart and Lackner (2013) | 40,000 | 5,274 | 10,183 | 40.43 | 8.285 |
| Own | 40,000 | 3,943 | 10,939 | 44.15 | 8.373 |

With both masses, the solutions obtained with our proposal outperform those obtained by other authors. This may be due to the precision of the identification model and the design of the optimization process (using genetic algorithms and optimizing both $k_T$ and $d_T$). It is worth noting that the suppression rate in the 20,000 kg case did not reach the performance of the TMD without stops (34.73 %). However, with 40,000 kg, the TMD with stops did surpass the unrestricted TMD solution by 4 %. These optimizations use the same resolution and limits as in case 1 (Table 5).

It is also interesting to analyze how the stroke affects the TMD performance in comparison with the TMD without stops. For this purpose, several optimizations were carried out, obtaining the best possible performance for different strokes (varying $X_s$ and $\text{stroke}_{\text{max}}$). The results for a TMD mass value of 40,000 kg are shown in Figure 6.

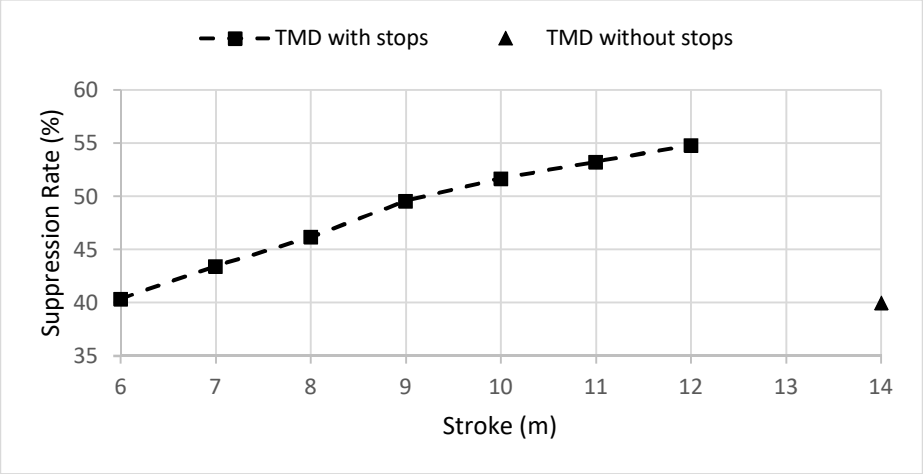


Figure 6. Suppression rate as a function of the stroke

Surprisingly, with this large TMD, the stops help to limit the TMD displacement along its track and also increase the suppression rate. The reason behind the vibration reduction when stops are limiting thr TMD stroke can be found through an analysis of the response in the frequency domain. Figure 7 shows the power spectral density of the TTD variable in three cases:

i) the baseline system without structural control (green),

ii) the system with TMD without stops (blue)

iii) the system with TMD with stops (red).

All these control solutions were tested for a TMD mass of 40,000 kg and an initial pitch angle of 5º for a time interval of 100 seconds.

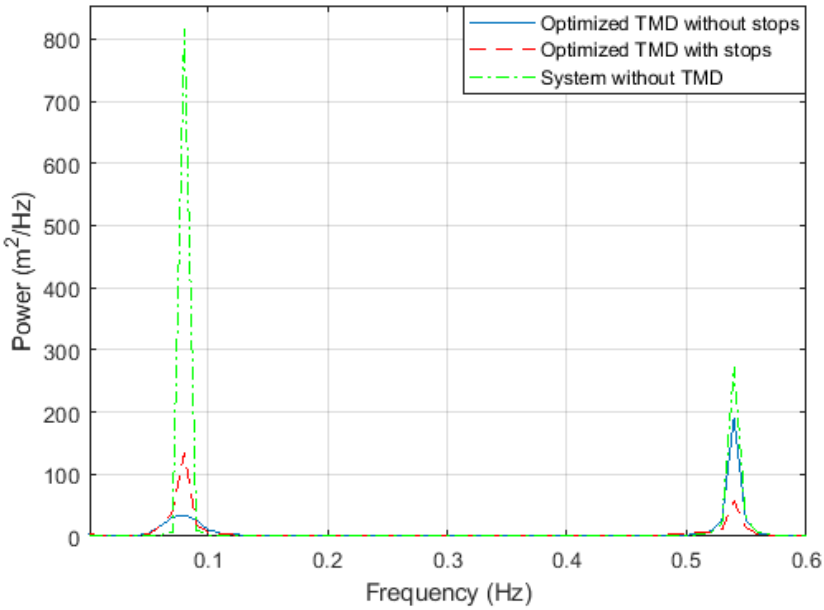


Figure 7. PSD of the TTD variable for the baseline system and the TMD solutions

The tower top displacement presents two modes, which correspond to the first and second collective platform pitch-tower bending modes, respectively. Both TMD solutions, with and without stops, are beneficial in reducing the system vibrations, but they achieve this objective in different ways. On one hand, the TMD without stops reduces significantly the first mode, which is the predominant one, to a magnitude lower than the second mode. On the other hand, the TMD with stops mitigates the first mode but it also reduces the second mode.

The response of the FOWT with both TMD solutions in the time domain is shown in Figure 8. The differences in performance (with and without stops) are evident; the TMD with stops reduces the second oscillation mode (high frequency) while the TMD without stops acts predominantly on the first mode (low frequency component).

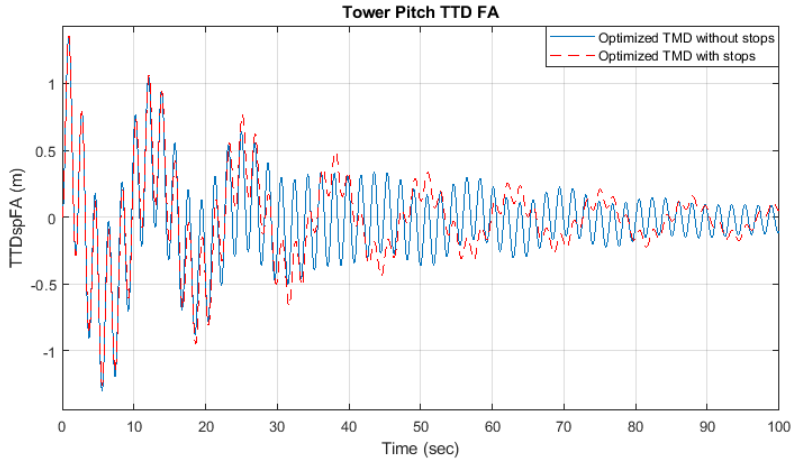


Figure 8. TTD of the floating wind turbine with TMD, with and without stops

According to the model of the system, the dynamics of the TMD with stops are different from the case of the TMD without them. This can be anticipated by observing the variation in the stiffness and damping parameters. With stops, the TMD spring stiffness is considerably lower since it is no longer the only responsible for stopping the oscillating mass. The damping coefficient is larger with stops, specifically in the case of 20,000 kg of TMD mass. Figure 9 shows the displacements (m) (top) and speeds (m/s) (bottom) of the TMD optimum solution, with and without stops, for a mass of 20,000 kg. These data were obtained by simulating a free decay test of 5 º platform pitch with FAST-SC for 100 seconds.

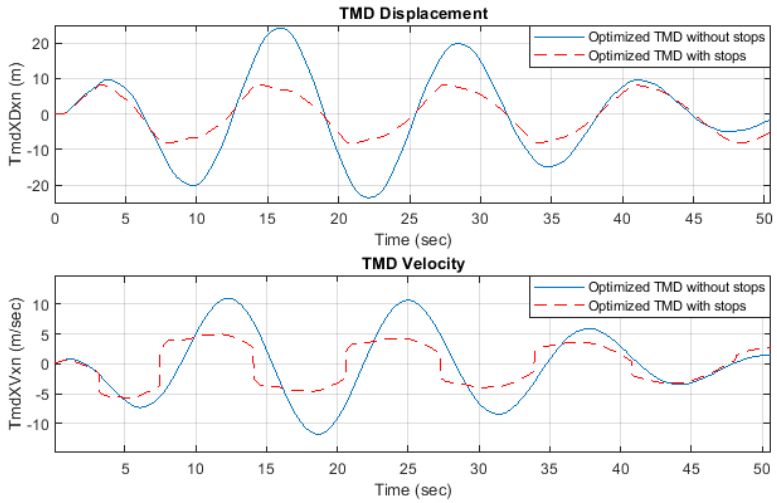


Figure 9. TMD displacement (top) and velocity (bottom), with (dashed red line) and without (blue line) stops

In addition to the reduction of TMD displacement, the change in the TMD velocity is noticeable (Figure 9, bottom). From a sinusoidal shape in the case of TMD without stops, it becomes a square waveform -of the same frequency- when stops are added. This may be because the stops induce an abrupt change of direction on the mass. The optimal solution with stops reaches a larger absolute average speed along the oscillation track, thus allowing the damper to absorb more energy.

### 5.3 Optimization case 3: TMD with optimized stops

Once the benefits of the addition of stops have been shown, their configuration is included in the optimization process to get the maximum vibration reduction. As already said, this adds three new variables to the optimization: the stops distance ($X_s$), the stops spring stiffness ($k_s$), and the stops damper coefficient ($d_s$).

The parameters obtained in this optimization case 3 are shown in Table 7, while the performance measures (suppression rate and stroke) of the TMD is shown in Table 8, along with the three other optimization cases for comparison purposes.

480 Table 7. Optimization case 3. Solutions

| $m_T$ (kg) | $k_T$ (N/m) | $d_T$ (Ns/m) | $X_s$ (m) | $k_s$ (N/m) | $d_s$ (Ns/m) |
|---|---|---|---|---|---|
| 20,000 | 1,877 | 6,174 | 8.09 | 502,900 | 893,400 |
| 40,000 | 2,197 | 11,614 | 8.00 | 499,600 | 315,200 |

481

482 Table 8. Performances comparison of all TMD configurations

| Configuration (case) | $m_T$ (kg) | *Suppression Rate* (%) | *Stroke* (m) |
|---|---|---|---|
| TMD w/o stops (1) | 20,000 | 34.24 | 23.6 |
| TMD w/ fixed stops (2) | 20,000 | 30.38 | 8.2 |
| TMD w/ optimized stops (3) | 20,000 | 31.88 | 8.2 |
| TMD w/o stops (1) | 40,000 | 40.00 | 14.3 |
| TMD w/ fixed stops (2) | 40,000 | 44.15 | 8.4 |
| TMD w/ optimized stops (3) | 40,000 | 44.79 | 8.4 |

483

484 In this third case, several optimizations were run, starting from low resolution -wider search space
485 (Table 9), and then moving on to a higher resolution –narrower search space (Table 10 and Table 11), with
486 different TMD masses.

487 Table 9. Low resolution - wide search limits configuration

| Variable | Resolution | Low limit | High limit |
|---|---|---|---|
| $k_T$ (N/m) | 10 | 100 | $10^5$ |

| | | | |
|---|---|---|---|
| $d_T$ (Ns/m) | 10 | 100 | $10^5$ |
| $X_s$ (m) | 0.1 | 9.0 | 5.0 |
| $k_s$ (N/m) | 100 | 100 | $10^6$ |
| $d_s$ (s/m) | 100 | 100 | $10^6$ |

488

489 Table 10. High resolution - narrow search limits configuration (20,000 kg)

| Variable | Resolution | Low limit | High limit |
|---|---|---|---|
| $k_T$ (N/m) | 1 | $10^3$ | $5 \cdot 10^3$ |
| $d_T$ (Ns/m) | 1 | $3 \cdot 10^3$ | $10^4$ |
| $X_s$ (m) | 0.01 | 7.80 | 8.30 |
| $k_s$ (N/m) | 100 | $10^4$ | $10^6$ |
| $d_s$ (s/m) | 100 | $10^4$ | $10^6$ |

490

491 Table 11. High resolution - narrow search limits configuration (40,000 kg)

| Variable | Resolution | Low limit | High limit |
|---|---|---|---|
| $k_T$ (N/m) | 1 | $10^3$ | $10^4$ |
| $d_T$ (Ns/m) | 1 | $10^3$ | $2 \cdot 10^4$ |
| $X_s$ (m) | 0.01 | 7.50 | 8.50 |
| $k_s$ (N/m) | 100 | $10^3$ | $10^6$ |

| | | | |
|---|---|---|---|
| $d_s$ (s/m) | 100 | $10^3$ | $10^6$ |

With the two different TMD masses considered, better solutions are obtained when optimizing the stops configuration. The improvement in terms of suppression rate, with respect to the fixed stop configuration (case 2) is 1.5 % and 0.64 % for TMD masses of 20,000 kg and 40,000 kg, respectively. Consequently, it is possible to conclude that the improvement provided by the stops' optimization increases with the stroke limitation with respect to the ideal TMD stroke without stops. This means that smaller/lighter TMDs, which require a longer stroke, will benefit more from the optimization of the stops' configuration.

## 6 Conclusions and future works

This paper addresses a real requirement of passive control. It is a step forward towards the design and implementation of devices that could reduce the impact of vibrations in floating wind turbines and that may attract industrial and commercial interest. In addition to this, exploring the use of these control devices will help reduce maintenance costs and increase the efficiency of floating wind turbines. The investigation on this solution not only fosters the use of renewable energies but proposing feasible solutions makes it more attractive and competitive for the wind industry.

The main contribution of this paper is to consider the stops that limit the stroke on a TMD control device to be included in an optimization loop. It has been proved that with this methodology good vibration suppression rates are achieved in comparison to cases that consider fixed stops or even without stops.

The optimization process of the stops, together with the TMD tuning parameters is advisable for any application that has to deal with strokes and mass constrains. These findings are not restricted to FOWT, but they can be applied to any other system to enhance the performance of passive structural TMD control.

Further studies could be focused on advanced structural control techniques, such as semi-active or active ones. Additionally, performing simulations under different wind and wave load conditions, as well as testing the proposals on real prototypes would be desirable. Finally, the use of more than one TMD acting cooperatively or being installed in different parts of the structure could be addressed.

**Funding**

This work was partially supported by the Spanish Ministry of Science, Innovation and Universities under MCI/AEI/FEDER Project number RTI2018-094902-B-C21.

**Author contributions**

**Villoslada, D.:** Conceptualization; Investigation; Software; Validation; Visualization; Writing - original draft. **Santos, M.:** Conceptualization; Investigation; Methodology; Funding acquisition; Writing - review & editing. **Tomás-Rodríguez, M.:** Conceptualization; Investigation; Methodology; Writing - review & editing.

**References**

Alonso-Zotes, F., Santos, M., 2017. Heuristic optimization of interplanetary trajectories in aerospace missions. Revista Iberoamericana de Automática e Informática Industrial 14(1), 1-15.

Caglayan, D. G., Ryberg, D. S., Heinrichs, H., Linßen, J., Stolten, D., & Robinius, M., 2019. The techno-economic potential of offshore wind energy with optimized future turbine designs in Europe. Applied Energy, 255, 113794.

Chen, X., Kareem, A., Xu, G., Wang, H., Sun, Y., & Hu, L., 2021. Optimal tuned mass dampers for wind turbines using a Sigmoid satisfaction function-based multiobjective optimization during earthquakes. Wind Energy.

Cong, C., 2019. Using active tuned mass dampers with constrained stroke to simultaneously control vibrations in wind turbine blades and tower. Advances in Structural Engineering, 22(7), 1544-1553.

Costoya, X., DeCastro, M., Carvalho, D., & Gómez-Gesteira, M., 2020. On the suitability of offshore wind energy resource in the United States of America for the 21st century. Applied Energy, 262, 114537.

Dinh, V. N., & Basu, B. 2015. Passive control of floating offshore wind turbine nacelle and spar vibrations by multiple tuned mass dampers. Structural Control and Health Monitoring, 22(1), 152-176.

539 Galán-Lavado, A., & Santos, M., 2021. Analysis of the effects of the location of passive control devices on
540 the platform of a floating wind turbine. Energies, 14(10), 2850.

541 He, E. M., Hu, Y. Q., Zhang, Y., 2017. Optimization design of tuned mass damper for vibration suppression
542 of a barge-type offshore floating wind turbine. Proc. of the Institution of Mechanical Engineers, Part
543 M: Journal of Engineering for the Maritime Environment, 231(1), 302-315.

544 Hu, Y., & He, E., 2017. Active structural control of a floating wind turbine with a stroke-limited hybrid
545 mass damper. Journal of Sound and Vibration, 410, 447-472.

546 Jonkman, J. M., & Buhl Jr, M. L., 2007. Loads analysis of a floating offshore wind turbine using fully
547 coupled simulation (No. NREL/CP-500-41714). National Renewable Energy Lab.(NREL), Golden,
548 CO (United States).

549 Jonkman, J. M., 2007. Dynamics modeling and loads analysis of an offshore floating wind turbine (No.
550 NREL/TP-500-41958). National Renewable Energy Lab.(NREL), Golden, CO (United States).

551 Jonkman, J., Butterfield, S., Musial, W., Scott, G., 2009. Definition of a 5-MW reference wind turbine for
552 offshore system development (No. NREL/TP-500-38060). National Renewable Energy Lab.(NREL),
553 Golden, CO (United States).

554 Lackner, M. A., & Rotea, M. A., 2011a. Structural control of floating wind turbines. Mechatronics, 21(4),
555 704-719.

556 Lackner, M. A., & Rotea, M. A., 2011b. Passive structural control of offshore wind turbines. Wind
557 energy, 14(3), 373-388.

558 Li, C., Zhuang, T., Zhou, S., Xiao, Y., & Hu, G., 2017. Passive vibration control of a semi-submersible
559 floating offshore wind turbine. Applied Sciences, 7(6), 509.

560 Liao, M., & Wu, Y., 2020. Conceptual design and dynamic analysis of a novel passive floating offshore
561 wind turbine structure. Ships and Offshore Structures, 1-10.

562 Mikati, M., Santos, M., & Armenta, C., 2013. Electric grid dependence on the configuration of a small-
563 scale wind and solar power hybrid system. Renewable energy, 57, 587-593.

564 Olondriz, J., Jugo, J., Elorza, I., & Aron Pujana-Arrese, S. A. Q., 2019. A feedback control loop
565 optimisation methodology for floating offshore wind turbines. Energies, 12(18), 3490.

566 Park, S., Lackner, M. A., Pourazarm, P., Rodríguez Tsouroukdissian, A., & Cross-Whiter, J., 2019. An
567 investigation on the impacts of passive and semiactive structural control on a fixed bottom and a
568 floating offshore wind turbine. Wind Energy, 22(11), 1451-1471.

569 Pimenta, F., Ruzzo, C., Failla, G., Arena, F., Alves, M., & Magalhães, F., 2020. Dynamic Response
570 Characterization of Floating Structures Based on Numerical Simulations. Energies, 13(21), 5670.

571 Rubio, P. M., Quijano, J. F., López, P. Z., 2019. Intelligent control for improving the efficiency of a hybrid
572 semi- submersible platform with wind turbine and wave energy converters. Revista Iberoamericana
573 de Automática e Informática Industrial 16(4), 480–491.

574 Saaed, T. E., Nikolakopoulos, G., Jonasson, J. E., Hedlund, H., 2015. A state-of-the-art review of structural
575 control systems. Journal of Vibration and Control, 21(5), 919-937.

576 Sierra-García, J.E., Santos M., 2020a. Performance analysis of a wind turbine pitch neurocontroller with
577 unsupervised learning. Complexity 2020 (2020).

578 Sierra-García, J.E., Santos M., 2020b. Exploring reward strategies for wind turbine pitch control by
579 reinforcement learning. Applied Sciences 10(21), 7462.

580 Sierra-García, J.E., Santos M., 2021. Neural networks and reinforcement learning in wind turbine
581 control. Revista Iberoamericana de Automática e Informática industrial, 18(4), 327-335.

582 Stewart, G., Lackner, M., 2013. Offshore wind turbine load reduction employing optimal passive tuned
583 mass damping systems. IEEE transactions on control systems technology, 21(4), 1090-1104. DOI:
584 10.1109/TCST.2013.2260825

585 Tomás-Rodríguez, M., & Santos, M., 2019. Modelling and control of floating offshore wind
586 turbines. Revista Iberoamericana de Automática e Informática industrial, 16(4), 381-390.

587 Vijfhuizen, W., 2006. Design of a wind and wave power barge. Universities of Glasgow and Strathclyde,
588 Glasgow, Scotland.

589 Villoslada, D., M. Santos, and M. Tomas-Rodriguez., 2020. Inerter-based Passive Structural Control for
590 Barge Floating Offshore Wind Turbines. IFAC-PapersOnLine 53.2: 12358-12363.

591 Villoslada, D., Santos, M., & Tomás-Rodríguez, M., 2021. General methodology for the identification of
592 reduced dynamic models of barge-type floating wind turbines. Energies, 14(13), 3902.

593 Wang, C. M., Utsunomiya, T., Wee, S. C., & Choo, Y. S., 2010. Research on floating wind turbines: a
594 literature survey. The IES Journal Part A: Civil & Structural Engineering, 3(4), 267-277.

595 Xie, S., Jin, X., & He, J., 2019a. Structural vibration control for the offshore floating wind turbine including
596 drivetrain dynamics analysis. Journal of Renewable and Sustainable Energy, 11(2), 023304.

597 Xie, S., Jin, X., He, J., & Zhang, C., 2019b. Structural responses suppression for a barge-type floating wind
598 turbine with a platform-based TMD. IET Renewable Power Generation, 13(13), 2473-2479.

599 Yang, W., Tian, W., Hvalbye, O., Peng, Z., Wei, K., & Tian, X., 2019a. Experimental research for
600 stabilizing offshore floating wind turbines. Energies, 12(10), 1947.

601 Yang, J., He, E. M., & Hu, Y. Q., 2019b. Dynamic modeling and vibration suppression for an offshore
602 wind turbine with a tuned mass damper in floating platform. Applied Ocean Research, 83, 21-29.

603 Yang, J. J., & He, E. M., 2020. Coupled modeling and structural vibration control for floating offshore
604 wind turbine. Renewable Energy, 157, 678-694.

605 Zuo, H., Bi, K., & Hao, H., 2020. A state-of-the-art review on the vibration mitigation of wind turbines.
606 Renewable and Sustainable Energy Reviews, 121, 109710.